Colloids and Surfaces B: Biointerfaces 72 (2009) 128–134

Contents lists available at ScienceDirect

Colloids and Surfaces B: Biointerfaces

journal homepage: www.elsevier.com/locate/colsurfb

Parameters governing gold nanoparticle X-ray radiosensitization of DNA in solution

Emilie Brun [a], Léon Sanche [b], Cécile Sicard-Roselli [a,*]

[a] Laboratoire de Chimie Physique, CNRS UMR 8000, Université Paris 11, Bât. 350, 91405 Orsay Cedex, France
[b] Groupe en Sciences des Radiations, Département de Médecine Nucléaire et Radiobiologie, Faculté de Médecine, Université de Sherbrooke, Sherbrooke, Quebec, J1H 5N4, Canada

ARTICLE INFO

Article history:
Received 11 January 2009
Received in revised form 26 March 2009
Accepted 26 March 2009
Available online 5 April 2009

Keywords:
Radiotherapy
Gold nanoparticles
Radiosensitization
DNA
X-ray irradiation

ABSTRACT

Radiosensitization by gold nanoparticles (GNP) is a promising approach for improving radiotherapy. We report herein the results of an investigation of three key-parameters governing such radiosensitization in DNA, namely, DNA:GNP molar ratio, GNP diameter and incident X-ray energy. We performed irradiations with a clinical orthovoltage source and tested concentration ratios up to 1:1, five sizes of GNP from 8 to 92 nm and six effective X-ray energies from 14.8 to 70 keV. The most efficient parameters are found to be large-sized GNP, high molar concentration and 50-keV photons, which could potentially result in a dose enhancement factor of 6. The relevance of such parameters as regards the development of future therapeutic applications is discussed. To the best of our knowledge, this study constitutes the first report of systematic data on radiosensitization by GNP.

1. Introduction

Cancer remains a major challenge in public health as it is still responsible for 25% of all deaths in western countries. Today, 60% of patients will go through irradiation treatment during their cancer history and roughly 50% during its early stage [1]. But as ionizing radiation does not discriminate between malignant and normal tissues, toxicity remains a dose-limiting factor despite the great efforts devoted to the improvement of the efficiency and tolerance of radiotherapy during these five decades. For example, dose fractionation, which is now a cornerstone, induces fewer side effects because it allows normal cells to repair their DNA lesions. Nevertheless, enhancing the radiation dose only to cancerous cells remains a goal which should considerably improve cancer treatment. Numerous chemical agents are presently being developed as potential radiosensitizers for hypoxic cells and several have undergone clinical trial [2,3] but their widespread use remains controversial. High atomic number material to enhance local dose delivery has also been known for a long time [4]. The first clinical observations of such a radiosensitization concerned head and neck cancer patients for whom necrosis and burning were noticed near metallic reconstructive plates after radiation therapy [5], this phenomenon being investigated *in vitro* later [6,7]. In these cases, radiosensitization was a major disadvantage.

Owing to advances in nanotechnology, it is now possible to draw benefit from this high-Z dose enhancement particularly through the accumulation of gold nanoparticles (GNP) in tumours. Gold seems to be the best candidate for this process because of its biocompatibility [8]. GNP have even been proposed as a reference nanoparticle system for low toxicity to use as a benchmark for comparison [9].

The first experimental evidence of the radiosensitizing effect of GNP was provided by Hainfeld et al. [10]. Intravenous injection of 1.9-nm diameter GNP into mammary tumour-bearing mice combined to 250 kVp X-rays resulted in a one-year survival of 86% versus 20% with X-rays alone. More recently, Chang et al. showed that, in a melanoma tumour-bearing mice model, 13-nm diameter GNP in conjunction with a single dose of 25 Gy from a 6 MeV electron beam led to a more pronounced reduction of the tumour volume than in the control groups [11]. A two-fold increase of apoptotic cells in animals treated with GNP and irradiation was achieved compared to irradiation alone. These pioneering results open the exciting perspective in oncology of a more efficient and specific radiotherapy treatment, although several key-parameters such as GNP synthesis, size and concentration, cancerous cell line, irradiation quality and energy were not similar. This reflects a lack of consensus and a need of standardization in order to determine the best conditions for medical application.

Understanding the role of GNP towards their potential molecular partners in the cell is a prerequisite for optimization and

* Corresponding author. Tel.: +33 1 69 15 61 77 32; fax: +33 1 69 15 61 88.
E-mail addresses: emilie.brun@lcp.u-psud.fr (E. Brun), sanche@usherbrooke.ca (L. Sanche), cecile.sicard@u-psud.fr (C. Sicard-Roselli).

0927-7765/$ – see front matter © 2009 Elsevier B.V. All rights reserved.
doi:10.1016/j.colsurfb.2009.03.025

application to therapy. Efforts have been made to identify the mechanisms responsible for radiosensitization by performing experiments with specific cell components: protein [12] and supercoiled DNA in solution [13–15] both irradiated with X-rays and in thin DNA films irradiated with high-energy electrons [16]. But the mechanism is not fully elucidated yet. It is known that interaction between X-rays and GNP results in the production of photo- and Auger electrons, and their secondaries of lower energy through energy loss processes. These latter carry most of the energy of the initial fast particle [17] and can induce DNA strand breaks very efficiently even below 15 eV [18]. All these electrons can interact with water to produce radicals – in other words, GNP can be seen as an additional $HO^{\bullet}$ source, as underlined by Carter et al. [14] – but they can also cause direct damage as proposed by Foley et al. and Zheng et al. [13,16]. Here also, comparing all these results is difficult because different systems were irradiated with particles of different sizes, different coatings and at different energies, so the impact of specific characteristics such as GNP coating or size cannot be extracted from them.

In our first approach to optimize the properties of GNP for radiosensitization, we focused on DNA. As the genome integrity keeper, this key molecule stands for a potential target for new treatments, that is why it is crucial to quantify its sensitivity to combined GNP and X-ray irradiation. In this paper, we report the results of investigation on the influence of GNP concentration, GNP size and incident effective X-ray energy on damage to plasmid DNA irradiated in solution. In each experiment, only one parameter was varied. From these results, we can suggest efficient conditions to obtain a significant damage enhancement. To the best of our knowledge, it is the first report of systematic data on radiosensitization by GNP.

2. Methods and materials

2.1. DNA preparation and manipulation

pGEM-3Zf(−) plasmid DNA (3197 bp, Promega) was extracted from *E. coli* $DH_{5\alpha}$ and purified with the QIAfilter Plasmid Giga Kit (Qiagen). Agarose gel electrophoresis showed that 95% of the extracted plasmid was in the supercoiled form. The DNA pellet was redissolved in TE buffer (10 mM Tris, 1 mM EDTA, pH 8) and desalted using Sephadex G-50 purification. The DNA concentration was obtained by measuring its absorption at 260 nm, taking a molar absorption coefficient of 5.3×10^7 L mol^{-1} cm^{-1} at pH 7.0. The stock solution concentration was approximatively 50 ng μL^{-1}.

2.2. Gold nanoparticles synthesis

All glassware used for GNP synthesis was thoroughly washed with aqua regia (3:1 HNO_3, HCl), rinsed extensively with water and oven-dried at 60 °C.

The colloidal GNP of 20- and 40-nm diameter were prepared by the original Turkevitch method [19]. Respectively, tri-sodium citrate dehydrate (1% (w/v), 26.4 or 4.2 mL) was added to an aqueous solution of $KAuCl_4$ (10^{-3} mol L^{-1}, 100 mL). The mixture was heated under moderate stirring for 10 min after the solution had turned purple.

Smaller particles were formed by the reduction of Au(III) by citrate in the presence of tannic acid as previously described [20]. It is considered that tannic acid reduces the chloroauric salts at the very beginning of the reaction forming nuclei and that citrate allows the growth once the nuclei has formed. $KAuCl_4$ aqueous solution (3×10^{-4} mol L^{-1}, 80 mL) and a reducing mixture consisting in citrate (1% (w/v), 4 mL), tannic acid (1% (w/v), 5 mL) and water (11 mL) were heated separately to 60 °C, then the latter solution was rapidly added to the former. Stirring and heating were carried out until 10 min after the colour change.

Larger particles were produced from 40-nm GNP seeds with ascorbic acid as a reductor by varying the ratio of seed to Au(III) as described in the following formula established by Turkevitch [21]:

$$D_f = D_{seed}\{([Au(0) + [Au(III)])/[Au(0)]\}^{1/3}$$

where D stands for the nanoparticle diameter. With ascorbic acid, no more nucleation occurs and all added Au(III) ions go into the shell growth. Ascorbic acid (10^{-2} mol L^{-1}) was added to a mixture of Au(III) (10^{-3} mol L^{-1}) and Au(0) (1.5×10^{-4} mol L^{-1} or 7×10^{-5} mol L^{-1}) under stirring at room temperature inducing an immediate colour change.

All nanoparticles obtained were subjected to several cycles of centrifugation to get rid of the excess of synthesis reactants and pellets of concentrated GNP were resuspended in water.

2.3. Gold nanoparticles characterization

All these nano-objects were thoroughly characterized by transmission electronic microscopy (TEM). Microscopy analyses were performed as follows: 10 μL droplet of the colloidal dispersions were cast onto formvar/carbon-coated copper grids (400 mesh) for a few minutes. Samples were imaged on a Philips CM120 transmission electron microscope operating at 80 kV. From the TEM images, the GNP diameter distribution was analysed with ImageJ software version 1.34 (at least 200 particles counted) [22].

To obtain the GNP concentrations, we proceeded as described in [23]. The experimentally determined molar absorption coefficients were extracted from the measured absorbance A by $A = \varepsilon \times l \times [GNP]$. GNP concentrations were determined from the number of moles of gold ions introduced for synthesis, assuming that all gold ions are reduced to form nanoparticles. We assumed a face-centered cubic organization of the nanoparticles, as in bulk gold, with 59 atoms nm^{-3} [24]. These concentration values corroborated those calculated from absorbance measurements and molar absorption coefficients at 450 nm published by Haiss et al. [25]. The molar absorption coefficients of the GNP at their respective absorption maxima were plotted against their volumes on a double logarithmic scale, exhibiting a linear dependence in agreement with the Mie theory (data not shown). The respective values are presented in Table 1.

2.4. Flocculation assay

Typically, GNP (700 μL, 0.05 nM final) were added to 200 μL of DNA in water with concentrations ranging from 0.05 to 50 nM. The mixture was incubated for different times from 5 min to overnight. Then, NaCl (100 μL, 10% (w/v) aqueous solution, i.e. 1.7 mol L^{-1}) was added to the solution to test for flocculation and absorbance was measured at 530 nm.

Table 1
Main characteristics of the GNP synthesized.

GNP diameter (nm)	8.1 ± 0.7	20.2 ± 3.0	37.5 ± 5.6	74.0 ± 11.9	91.7 ± 16.5
Plasmon resonance wavelength (nm)	520 (weak)	520	529	540	548
Molar absorption coefficient (L mol^{-1} cm^{-1})	6.1×10^7	1.4×10^9	6.8×10^9	6.3×10^{10}	1.0×10^{11}

Table 2
Parameters of the superficial therapy X-ray unit.

Effective energy (keV)	Filtration (mm)	Potential energy (kVp)	Filament current (mA)	Surface dose rate (Gy min^{-1})	Mean to surface dose rate ratios
14.8	0.4 Al	30	7.6	2.31	0.875
24.4	0.8 Al	80	3.9	2.76	0.955
29.8	2.0 Al	80	7.9	2.81	0.972
42.4	1.8 Al + 0.1 Cu	100	10.4	2.70	0.981
49	1.1 Al + 0.3 Cu	120	11.1	2.46	0.983
70.1	0.2 Al + 1.0 Cu	150	13.1	2.52	0.992

2.5. X-ray irradiation

Irradiations were performed in Lindemann capillary tubes (Specialglass capillaries, 1.5-mm diameter, 0.01-mm thick inner wall, Glas Tecnik&Konstruktion, Germany). X-rays of different effective energies were generated with a superficial therapy X-ray unit (Pantak Therapax 3 series) at the Université de Sherbrooke Hospital Center. This type of orthovoltage source does not produce monochromatic X-rays but an intense peak at an energy determined by a filter (see Table 2) with a broad, smoothly varying bremsstrahlung background. Such an X-ray spectrum has been simulated by McMahon et al. [26]. Samples were exposed at 15 cm from the source with a treatment cylinder of 2.5-cm diameter. The dose rates at the incident surface of the samples were measured with an ionization chamber (NE 2571 and/or NE 2536/3C) including corrections for temperature, pressure and backscattering. They can be found in Table 2. Corrections were also made for the variation in X-ray intensity across the sample. The mean absorbed dose rate D_m, in a sample of density ρ and thickness x, was calculating from the dose rate at the surface, D_s, according to:

$$D_m = D_s \frac{1 - e^{-(\mu/\rho)\rho x}}{(\mu/\rho)\rho x} \quad (1)$$

The proportionality factors between D_m and D_s for each effective energy can be found in Table 2.

2.6. Agarose gel electrophoresis

The different plasmid DNA configurations were resolved as previously described [27]. The relative amounts of each form of DNA were obtained from ImageJ analysis. To correct for the weaker binding of SYBR Green I to the supercoiled form of DNA compared to nicked circular and linear configurations, supercoiled DNA was digested by the ECOR1 enzyme in appropriate buffer at 37 °C during 45 min resulting in its linearization. The same amounts of supercoiled and digested plasmid were loaded on an agarose gel, stained as usual. A factor of 1.2 was found between the areas under the peaks after quantification with ImageQuaNT TL software (Molecular Dynamics).

3. Results and discussion

3.1. GNP characterization

Among the multiple synthesis routes available to generate GNP [28], we focused on different procedures leading to very good

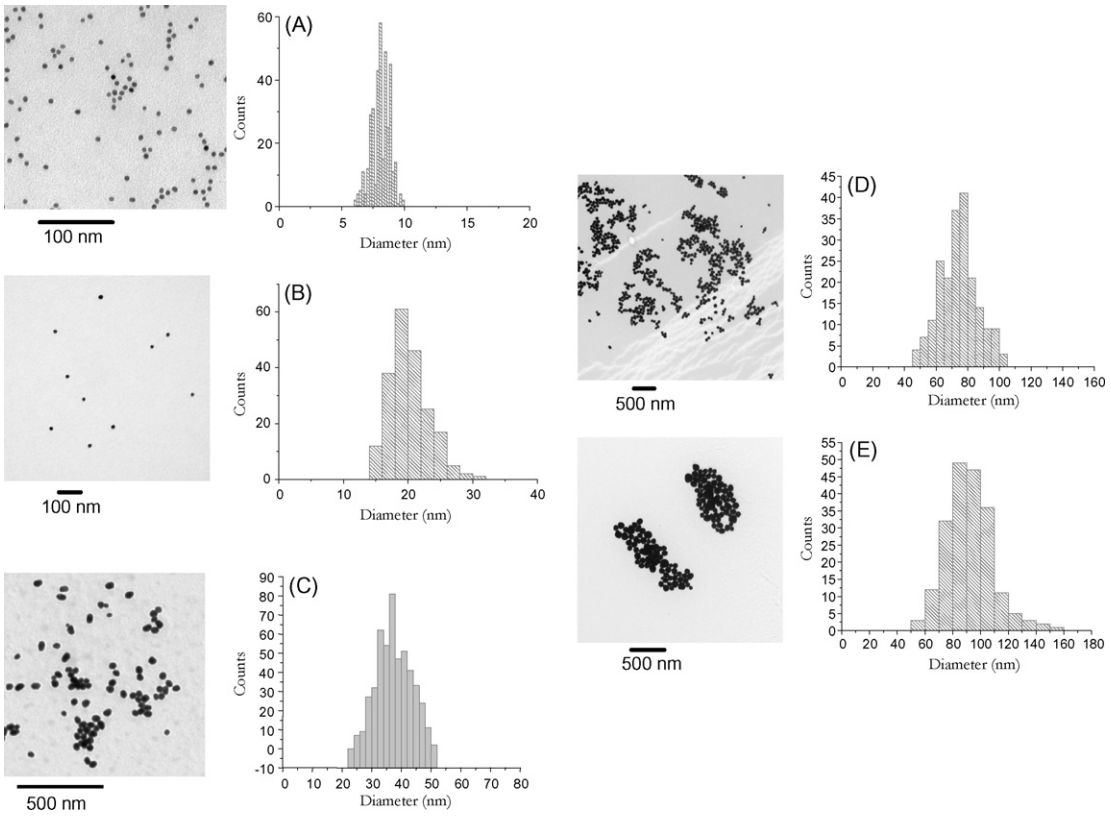

Fig. 1. TEM images and size distributions of all gold nanoparticles synthesized. Mean sizes are respectively A: 8.1 ± 0.7 nm, B: 20.2 ± 3.0 nm, C: 37.5 ± 5.6 nm, D: 74.0 ± 11.9 nm and E: 91.7 ± 16.5 nm.

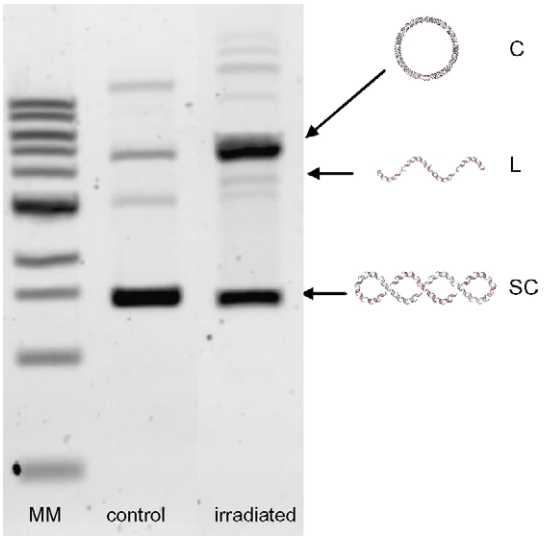

Fig. 2. Typical agarose gel electrophoresis of DNA. MM: mass marker; control: 100 ng of DNA were deposited onto the well, the major conformation being the supercoiled form; irradiated: 100 ng of DNA irradiated with 49 keV effective X-rays in solution in the presence of one GNP per plasmid were loaded. The irradiation dose was 3.6 Gy. The remarkable forms are C: circular, L: linear, SC: supercoiled.

homogeneities of sizes. Gold particles with diameters ranging from 8 to 92 nm were thus obtained. Fig. 1 shows representative TEM images and the corresponding size distribution histograms. In all five cases, more than 200 objects were counted. Micrographs clearly revealed that gold colloids were effectively spherically shaped and well-dispersed. With tannic acid, 8.1 ± 0.7 nm GNP were produced. With the Turkevitch protocol, we obtained sizes of 20.2 ± 3.0 and 37.5 ± 5.6 nm. Seeds and ascorbic acid allowed the syntheses of 74.0 ± 11.9 and 91.7 ± 16.5 nm GNP (Table 1). Prior to use, all nanoparticles were washed by repeated cycles of centrifugation in order to get rid of the excess of reactants and to minimize a possible coating effect. To check the absence of any aggregation resulting from washings, UV–visible spectra were recorded before and after centrifugation: in all cases, the plasmon resonance band shape and position remained unchanged. Thus, the only variable parameter between GNP populations was their mean diameter. As suggested by the group of Drezek, such a consistent report in the physico-chemical properties of nanomaterials is essential for cross comparison of data [9].

3.2. DNA–GNP interaction

Plasmid DNA pGEM-3Zf(−) was chosen because its degradation pattern was previously described [27]. The interaction between DNA and GNP was then evaluated. To probe their potential affinity, we performed flocculation assays. In general, addition of electrolytes (10% NaCl) causes aggregation of GNP because it shields the repulsive double-layers charges [29]. But a steric protection can be obtained with polymers [30], thiolated oligonucleotides [31] or proteins [12] interacting with GNP. In our case, whatever the DNA:GNP ratio, up to 1000:1, and incubation time, flocculation was not prevented after addition of NaCl, testifying of the absence of strong interaction between the two partners as already reported [32]. As their surface was not functionalized after synthesis, GNP possess a negative charge due to some remaining citrate ligands, whatever the synthesis way was. Repulsive interaction is then expected with phosphate groups of DNA backbone. As several studies showed that a covalent bond is not necessary to generate a radio-enhancement [12,15], we then proceeded to irradiation experiments.

3.3. Irradiation experiments

In this study, we probed the dependence of radiosensitization on DNA:GNP ratio, GNP size and incident photon energy. Damage enhancement measurements for effective X-ray energies ranging from 10 to 80 keV were performed with a tuneable therapeutic source. When investigating the impact of the GNP concentration and of effective X-ray energy, we focused on a single size: 37.5-nm GNP. We have previously described the radiosensitizing effect of 40-nm diameter GNP on the protein human centrin 2 [12] and on bacteria [33]. The interest for this range of size stems from its biological relevance. Indeed, Chithrani et al. showed a preferential penetration of 50-nm diameter GNP in HeLa cells [34]. So, except specifically mentioned, experiments were conducted with 37.5-nm GNP.

3.3.1. Influence of DNA:GNP ratio

In a first step, we focused on the DNA:GNP ratio influence. Stock water solutions of DNA and of concentrated GNP were mixed 30 min prior to X-rays exposure, resulting in aerated solutions with final concentrations of 5 nM for DNA and from 0 to 5 nM for GNP, which corresponds to 0.15% of gold by weight. Irradiations were achieved by a superficial therapy unit (Pantak Therapax 3 series) producing 49 keV effective X-rays in this case. The different forms of plasmid DNA were resolved by a 1% agarose gel electrophoresis and quantified with ImageJ software [22]. When the supercoiled plasmid (SC) undergoes a single-strand break (SSB), a topological change occurs causing the molecule to adopt a circular form. Typically, a double-strand break (DSB) within 10 adjacent base pairs causes DNA to become linear. A typical electrophoresis gel is presented in Fig. 2. Non-irradiated samples mainly consisted of supercoiled DNA; the circular form accounts for ∼5%. Other bands were present, to a far lesser extent, identified as concatemeric and cross-link forms [27]. After irradiation, proportion of the supercoiled DNA was drastically diminished, mainly in favour of the circular form. This SC decrease is reported in Fig. 3A for all GNP concentrations. Different DNA:GNP ratios were explored up to one nanoparticle per plasmid. In all cases, the percentage decrease of the SC form was proportional to the dose. As already observed for the human centrin 2 protein [12], the higher the number of GNP, the higher the enhancement. To quantify this effect, a dose enhancement factor (EF) was defined as the ratio between the slopes of the linear fits derived from the percentage of SC as a function of the dose with and without GNP. In Fig. 3B, EF is plotted with respect to the GNP concentration. From 1 up to 5 nM, corresponding to a 1:1 ratio, it varies linearly with the GNP concentration. Interestingly, even for 10 plasmids, i.e. more than 30,000 bp per GNP, we obtained a significant dose enhancement factor of 1.6 ± 0.3. For the 1:1 ratio, it raises up to 3.3 which means that in the presence of GNP, only 30% of the dose is necessary to induce an equivalent damage. For DNA films bombarded with 60 keV electrons, Zheng et al. obtained an EF for SC loss of 1.5 when DNA:GNP ratio was 1:1 [16] and Foley et al. reported a maximum enhancement of ∼2 for a 1:100 ratio [13]. Besides, a two-fold enhancement is unanimously reported in theoretical works using conventional orthovoltage sources and a tissue loading of 0.5–1% by weight [35]. So, our experimental conditions result in a very high efficiency.

3.3.2. Influence of GNP size

As already mentioned, in the emerging studies of radiosensitization by GNP of different characteristics, on isolated molecules, cells or animals, the most obvious difference was their size. Previous works focused on GNP of diameters varying from 1.9 [10] to 12 nm [11] but not beyond, despite experimental proof of the biological relevance of bigger nano-objects [34]. Besides, cytotoxicity seems to depend also on GNP size [36]. Pan et al. showed that in four

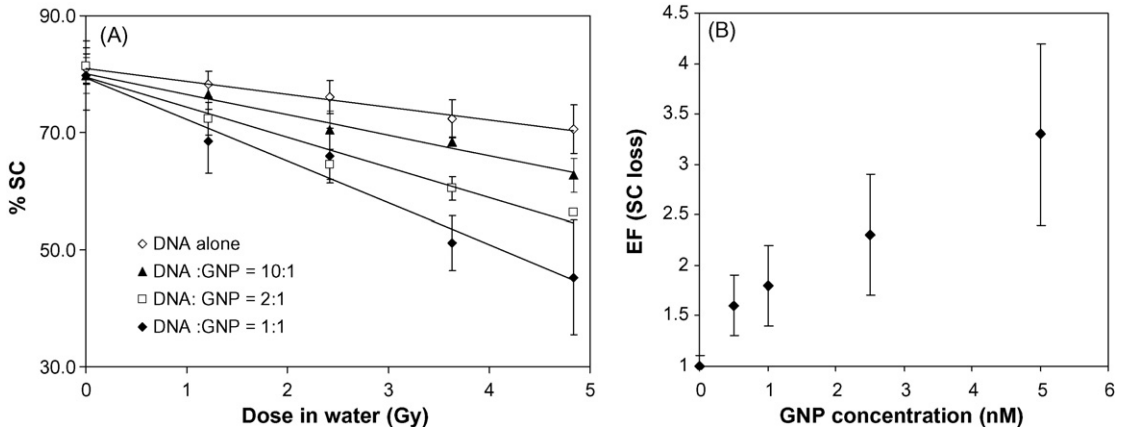

Fig. 3. Influence of the GNP concentration. (A) Loss of supercoiled DNA versus the dose in water for different GNP concentrations. The concentration of DNA was 5 nM, and that of the GNP varied from 0 to 5 nM. Irradiations were performed with 49 keV effective X-rays. Experiments were repeated three times and the reported values are the average of the three quantifications. Error bars are standard deviations. (B) Dose enhancement factor (EF) for the loss of supercoiled DNA versus GNP concentration. EF is obtained *via* the graphs represented in A. It is the ratio between the slopes of the linear fits derived from the percentage of SC as a function of the dose with and without GNP.

different cell lines, GNP of 1.4-nm diameter admitted the highest toxicity. So when investigating the impact of GNP sizes on the EF, we focused on GNP with diameters from 8 to 92 nm. We carried on these experiments with a DNA:GNP ratio of 5:1 and 49 keV effective X-rays energy. Of course, these results are pertinent in so far as we produced GNP highly controlled in size and we determined thoroughly size distributions. For each size, the dependence of SC loss with the dose was plotted for 0–5 Gy, each point being the average of three independent experiments as can be seen in Fig. 4A. Here also, data were fitted linearly to obtain the slopes, the resulting EF are presented in Fig. 4B. We obtain a linear relationship between the enhancement factors obtained for the SC loss and the GNP diameter. When GNP diameter was increased from 8 to 92 nm, the EF raised to 3.0. As the EF does not vary with GNP radius to the power three, the number of gold atoms is not the only parameter governing the effect of GNP diameter on radiosensitization. Geometry and confinement must be considered. From our *in vitro* study we can conclude that the largest GNP gave the highest EF.

3.3.3. *Influence of effective incident X-ray energy*

The choice of optimal beam energy is an important consideration in radiotherapy. In literature, two concepts have been advanced to predict the optimal energy for irradiating tumours loaded with high-Z elements. On the one hand, irradiation with an energy just above the K-edge had been a first conceptual approach to profit from the contribution of the Auger events. But experimentally, combination of *cis*-diamminedichloroplatinum (II) treatment and synchrotron irradiations on rat F98 glioma cells below and above the K-edge of platinum (78.4 keV) result in identical damages [37]. As underlined by Hainfeld et al. in a recent review [38], such an incident photon with the energy of the edge will spend all its energy to eject an electron from the K-shell. This photoelectric electron will not receive much kinetic energy and so will not help in propagating the damages. On the other hand, it has been suggested to take into account the difference in absorption between the high-Z element and its environment. Corde et al. irradiated carcinoma cells pre-exposed to iodo-deoxyuridine during 48 h with the monochromatic X-ray beam of the European Radiation Synchrotron Facility [39]. They found that the minimum survival was not obtained just above the K-edge of I (33.2 keV) but at 50 keV. To explain these observations, it is valuable to consider the parameter μ_{en}/ρ which is the mass energy absorption coefficient, and which quantifies the energy actually deposited in a local volume. μ_{en}/ρ values, available at the National Institute of Standards and Technology, allows to plot, as in Fig. 5, the ratio between mass energy absorption coefficients of gold and water. A theoretical maximum EF is found between 40 and 50 keV, with a bell-shaped behaviour. So we proposed to explore the influence of the effective incident X-ray energy on the radiosensitization by GNP experimentally.

We proceeded to irradiations with six different energies with comparable dose rates. These measurements were made with GNP of 37.5-nm diameter and a DNA:GNP ratio of 1:1. Once again, quantification of electrophoresis gel allowed the SC degradation quantification. Fig. 6 depicts the variation of the EF with respect to the effective X-ray energies. Here also, the data were obtained from the slopes of %SC versus dose curves, each point corresponding to

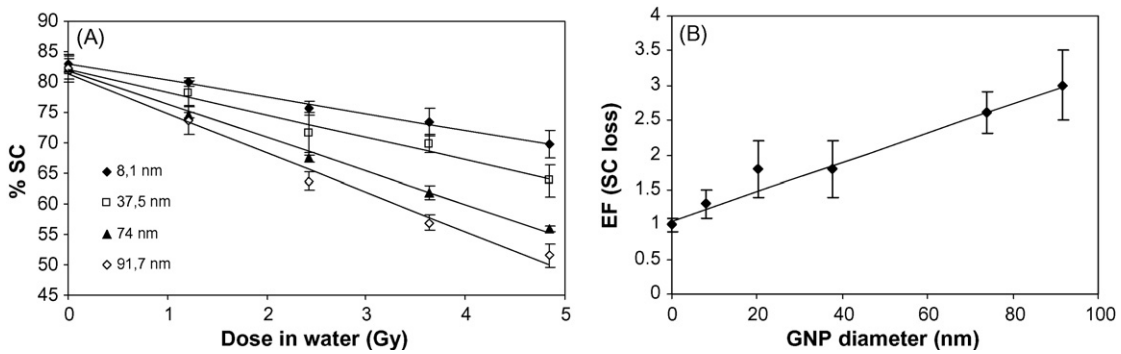

Fig. 4. Influence of the GNP size. (A) Loss of supercoiled DNA versus the dose in water for different GNP sizes. The DNA:GNP ratio was 5:1. Effective X-ray energy was 49 keV. Experiments were repeated three times and the reported values are the average of the three quantifications. Error bars are standard deviations. (B) Dose enhancement factor versus GNP diameter. The linear regression coefficient R^2 was 0.9962. Error bars are standard deviations of three independent experiments.

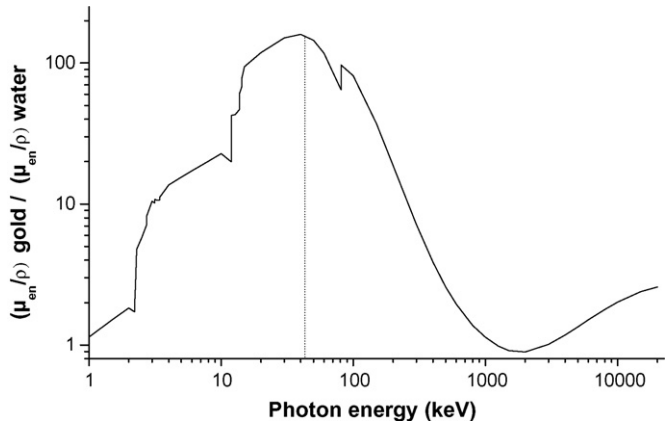

Fig. 5. Ratio between μ_{en}/ρ of gold and of water versus the X-ray energy.

a triplicate. Because of high standard deviations, we cannot clearly conclude as regards the presence of a maximum around 40–50 keV. As it is well-established that X-rays generate HO• radicals in water, we compared this pattern with the rate of formation of HO• versus incident X-ray energy. It is interesting to note that hydroxyl radical yields dependence on photon energy does not exhibit a similar variation [40]. Effectively, G(HO•) increases linearly with X-ray energy, from 0.20 to 0.23 μmol J^{-1} from respectively 20 to 100 keV. So the dependence of EF versus X-ray energy does not seem to be governed mainly by different production rates of hydroxyl radicals but by the presence of GNP.

3.3.4. Perspectives for therapy

From all these experiments, a significant dose enhancement with GNP could be obtained with a high concentration and a large diameter of GNP irradiated with 50 keV X-rays. Assuming independence of these parameters, a potential factor of ~6 may be under reach for 92-nm diameter GNP with a 1:1 DNA:GNP ratio and 50 keV. This opens the perspective of a huge reduction of doses delivered to patients with an equally efficient treatment and much less side effects, all the more so GNP are biocompatible. Besides, the National Institute of Standards and Technology has issued gold spheres of 10, 30 and 60 nm in diameter as its first reference standards of non-toxicity [41].

However, in terms of medical application, a compromise will have to be reached. Indeed, several constraints as regards GNP size and surface emerge from the translation of this promising area of research to therapy because these factors govern their metabolism, distribution and internalization. One of the most attractive routes for delivery is intravenous injection. When injected to the bloodstream, GNP must escape the reticulo-endothelial system and

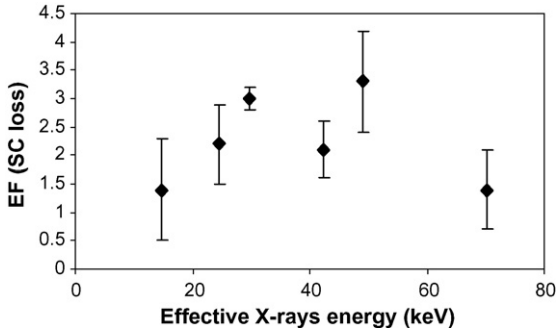

Fig. 6. Influence of the X-ray energy. Dose enhancement factor versus effective X-ray energy. GNP had a 37.5-nm diameter. The DNA:GNP ratio was 1:1. Error bars are standard deviations of three independent measurements.

their subsequent uptake by macrophages. Increasing their half-life in blood circulation is an absolute prerequisite for targeting the tumours. Particles with a diameter ≥200 nm activate the complement system more efficiently, are more easily opsonized and as a result are cleared faster, which imposes a higher size limit [42]. Then, to concentrate GNP specifically on tumours, passive or active targeting can be achieved. Passive targeting relies on special properties of solid tumours: they are characterized by an extra-vascularization, angiogenesis, which plays a major role in the growth and spread of cancer, and a leaky vasculature. This is the so-called enhanced permeability and retention effect GNP can take advantage of to preferentially accumulate in cancerous cells on condition they can penetrate blood vessel pores. In tumours, the fenestration increases from 10 nm up to 1 μm and this enlargement is accompanied with a 40-fold reduction in transmembrane electrical resistance [42]. Once in the nearby of tumoural tissue, GNP must be sufficiently small to enter cancer cells, for example by diffusion [43] or receptor-mediated endocytosis [44], which means a diameter <100 nm. If the nucleus proves to be the best target for GNP, a more drastic constraint is imposed since import through nuclear pores is only possible below 30-nm diameter. Thus the nanoparticles size is of great importance as regards cell penetration but it also influences their biodistribution.

In fact, for non-functionalized GNP, biodistribution studies in mice or rats 24 h after intravenous injection revealed high gold concentrations in liver, lung, spleen, and kidney, the smallest GNP showing the most sprawling distribution [45,46]. When the particle size increases, the concentration in spleen increases whereas the concentration in lung decreases. Interestingly, 50-nm GNP are largely distributed and are able to pass the blood-brain barrier [46]. But to provide an efficient treatment, it is highly important to go beyond these biodistributions and to address GNP to specific cell types and compartments. As GNP are versatile platforms, it is possible to conjugate them to molecules of interest such as antibodies [47] or nuclear localization signal peptides [48]. In all cases, the strategy to follow will strongly depend on the characteristics and localization of the cells to target [49].

Concerning present radiotherapeutic modalities, a number of considerations must also be taken into account. In its infancy, radiotherapy treatment was administered with such orthovoltage range X-ray sources. But the dose distribution profile was problematic with a high superficial dose at the skin entrance and an exponential decrease with depth. Nowadays, except for superficial skin cancers, radiotherapeutic X-rays are produced by electron linacs. But, as can be seen in Fig. 5, in this MeV region, there is little or no difference in absorption coefficients between gold and soft tissues. However, in this energy range, the primary interaction produces mostly Compton electrons with a wide but lower energy range in the sub MeV region [50]. Gold has a mass absorption coefficient for such electrons that can be an order of magnitude larger than that of biological matter. This consideration shows that the secondary electrons produced by the primary event would interact preferentially with GNP. Thus, with clinical photons, radiosensitization is still expected but arising from secondary species. Indeed, McMahon et al. found that the combination of GNP and kilovoltage sources presented an advantage over linac devices [26]. So with regards to GNP radiosensitizing effect, it may be of interest to examine some possibilities of refinement of existing X-ray sources or development of new ones with endoscopic abilities (e.g. explore the fabrication of insertable miniature X-ray tubes). Sources inside needles or flexible catheters are currently under development [51]. Their energy range (40–50 keV) would suit perfectly GNP mass coefficient absorption and the resulting low penetration power would be overcome by their insertion in the body. They could also be used with laparoscopy to access deep-buried tumours. Another interesting feature would be to provide X-ray conventional sources with

IMRT capabilities in order to improve the dose localization and bypass the initial default previously cited.

4. Conclusions

Undoubtedly GNP are promising tools for radiotherapy. More than a proof-of-principle, we identified for the first time three key-parameters governing their radiosensitizing effect: their concentration, their size and X-ray incident energy. In our conditions, the most efficient parameters are large-sized GNP, high concentration and 50-keV photons. We confronted them to those required for clinical therapeutic applications. With advances in instrumentation and miniaturization, 50-nm diameter GNP specially designed to target cancerous cells associated with orthovoltage X-ray irradiation could be a new weapon in the war against cancer.

Acknowledgements

We thank Ariane Dumont for providing us with the plasmid, Pierre Cloutier for technical assistance, Danielle Jaillard (Centre Commun de Microscopie Electronique d'Orsay) for her help in TEM experiments and Luc Ouellet for helpful discussion. This work was supported by the Canadian Institutes of Health Research (CIHR) and the Centre National de la Recherche Scientifique (CNRS).

References

[1] A. Jemal, R. Siegel, E. Ward, Y. Hao, J. Xu, T. Murray, M.J. Thun, CA Cancer J. Clin. 58 (2008) 71.
[2] Y. Shibamoto, L. Zhou, H. Hatta, M. Mori, S.I. Nishimoto, Int. J. Radiat. Oncol. Biol. Phys. 49 (2001) 407.
[3] K. Miyake, M. Shimada, M. Nishioka, K. Sugimoto, E. Batmunkh, Y. Uto, H. Nagasawa, H. Hori, Cancer Lett. 272 (2008) 325.
[4] F.W. Spiers, Br. J. Cancer 22 (1949) 521.
[5] M.H. Castillo, T.M. Button, R. Doerr, M.I. Homs, C.W. Pruett, J.I. Pearce, Am. J. Surg. 156 (1988) 261.
[6] D.F. Regulla, L.B. Hieber, M. Seidenbusch, Radiat. Res. 150 (1998) 92.
[7] D. Regulla, E. Schmid, W. Friedland, W. Panzer, U. Heinzmann, D. Harder, Radiat. Res. 158 (2002) 505.
[8] R. Shukla, V. Bansal, M. Chaudhary, A. Basu, R.R. Bhonde, M. Sastry, Langmuir 21 (2005) 10644.
[9] N. Lewinski, V. Colvin, R. Drezek, Small 4 (2008) 26.
[10] J.J. Hainfeld, D.N. Slatkin, H.M. Smilowitz, Phys. Med. Biol. 49 (2004) N309.
[11] M. Chang, A. Shiau, Y. Chen, C. Chang, H. Chen, C. Wu, Cancer Sci. 99 (2008) 1479.
[12] E. Brun, P. Duchambon, Y. Blouquit, G. Keller, L. Sanche, C. Sicard-Roselli, Rad. Phys. Chem. 78 (2009) 177.
[13] E.A. Foley, J.D. Carter, F. Shan, T. Guo, Chem. Commun. 25 (2005) 3192.
[14] J.D. Carter, N.N. Cheng, Y. Qu, G.D. Suarez, T. Guo, J. Phys. Chem. B 111 (2007) 11622.
[15] K.T. Butterworth, J.A. Wyer, M. Brennan-Fournet, C.J. Latimer, M.B. Shah, F.J. Currell, D.G. Hirst, Radiat. Res. 170 (2008) 381.
[16] Y. Zheng, D.J. Hunting, P. Ayotte, L. Sanche, Radiat. Res. 169 (2008) 19.
[17] S. Uehara, H. Nikjoo, D.T. Goodhead, Radiat. Res. 152 (1999) 202.
[18] B. Boudaiffa, P. Cloutier, D. Hunting, M.A. Huels, L. Sanche, Science 287 (2000) 1658.
[19] J. Turkevitch, P.C. Stevenson, J. Hillier, Discuss. Faraday Soc. 11 (1951) 55.
[20] G. Tsutsui, S. Huang, H. Sakaue, S. Shingubara, T. Takahagi, Jpn. J. Appl. Phys. 40 (2001) 346.
[21] J. Turkevitch, Gold Bull. 18 (1985) 86.
[22] M.D. Abramoff, P.J. Magelhaes, S.J. Ram, Biophotonics Int. 11 (2004) 36.
[23] S. Link, M.A. El-Sayed, J. Phys. Chem. B 103 (1999) 8410.
[24] C. Kittel, Introduction to Solid-State Physics, 7th Ed., Wiley, New-York, 1996.
[25] W. Haiss, N.T. Thanh, J. Aveyard, D.G. Fernig, Anal. Chem. 79 (2007) 4215.
[26] S.J. McMahon, M.H. Mendenhall, S. Jain, F. Currell, Phys. Med. Biol. 53 (2008) 5635.
[27] Z. Cai, P. Cloutier, L. Sanche, D. Hunting, Radiat. Res. 164 (2005) 173.
[28] M.C. Daniel, D. Astruc, Chem. Rev. 104 (2004) 293.
[29] J.N. Israelachvili, Intermolecular and Surface Forces, Academic Press, London, 1992.
[30] P.G. De Gennes, Adv. Colloid Interface Sci. 27 (1987) 189.
[31] Y. Chen, J. Aveyard, R. Wilson, Chem. Commun. (Camb) 24 (2004) 2804.
[32] H. Li, L. Rothberg, Proc. Natl. Acad. Sci. USA 101 (2004) 14036.
[33] A. Simon-Deckers, E. Brun, B. Gouget, M. Carrière, C. Sicard-Roselli, Gold Bull. 41 (2008) 187.
[34] B.D. Chithrani, A.A. Ghazani, W.C. Chan, Nano Lett. 6 (2006) 662.
[35] S.H. Cho, Phys. Med. Biol. 50 (2005) N163.
[36] Y. Pan, S. Neuss, A. Leifert, M. Fischler, F. Wen, U. Simon, G. Schmid, W. Brandau, W. Jahnen-Dechent, Small 3 (2007) 1941.
[37] M.C. Biston, A. Joubert, J.F. Adam, H. Elleaume, S. Bohic, A.M. Charvet, F. Esteve, N. Foray, J. Balosso, Cancer Res. 64 (2004) 2317.
[38] J.F. Hainfeld, F.A. Dilmanian, D.N. Slatkin, H.M. Smilowitz, J. Pharm. Pharmacol. 60 (2008) 977.
[39] S. Corde, A. Joubert, J.F. Adam, A.M. Charvet, J.F. Le Bas, F. Esteve, H. Elleaume, J. Balosso, Br. J. Cancer 91 (2004) 544.
[40] J. Fulford, P. Bonner, D.T. Goodhead, M.A. Hill, P. O'neill, J. Phys. Chem. A 103 (1999) 11345.
[41] W. Jahnen-Dechent, U. Simon, Nanomedicine 3 (2008) 601.
[42] D.F. Emerich, C.G. Thanos, Biomol. Eng. 23 (2006) 171.
[43] N. Pernodet, X. Fang, Y. Sun, A. Bakhtina, A. Ramakrishnan, J. Sokolov, A. Ulman, M. Rafailovich, Small 2 (2006) 766.
[44] B.D. Chithrani, W.C. Chan, Nano Lett. 7 (2007) 1542.
[45] W.H. De Jong, W.I. Hagens, P. Krystek, M.C. Burger, A.J. Sips, R.E. Geertsma, Biomaterials 29 (2008) 1912.
[46] G. Sonavane, K. Tomoda, K. Makino, Colloids Surf. B Biointerfaces 66 (2008) 274.
[47] I.H. El-Sayed, S. Huang, M.A. El-Sayed, Cancer Lett. 239 (2006) 129.
[48] A.G. Tkachenko, H. Xie, Y. Liu, D. Coleman, J. Ryan, W.R. Glomm, M.K. Shipton, S. Franzen, D.L. Feldheim, Bioconjug. Chem. 15 (2004) 482.
[49] M.S. Muthu, S. Singh, Nanomedicine 4 (2009) 105.
[50] H.E. Johns, J.R. Cunningham, The Principles of Radiology, C.C. Thomas Publisher, USA, 1983.
[51] G. Gutman, E. Sozontov, E. Strumban, F.F. Yin, S.W. Lee, J.H. Kim, Phys. Med. Biol. 49 (2004) 4677.